

Lepton Flavor Violation in Nonholomorphic Soft SUSY-Breaking Scenarios: Experimental Limits and Excesses

M. REHMAN^{1*} AND S. HEINEMEYER^{2†}

¹*Department of Physics, Comsats University Islamabad, 44000 Islamabad, Pakistan*

²*Instituto de Física Teórica, (UAM/CSIC), Universidad Autónoma de Madrid, Cantoblanco, 28049 Madrid, Spain*

Abstract

We investigate the prospects for the observation of lepton flavor violation (LFV) within the nonholomorphic supersymmetric standard model (NHSSM). We examine charged lepton flavor-violating (cLFV) decays such as $\mu \rightarrow e\gamma$, $\tau \rightarrow e\gamma$ and $\tau \rightarrow \mu\gamma$ to impose indirect constraints on both LFV holomorphic and nonholomorphic (NH) soft Supersymmetry-breaking (SSB) terms. These constraints are subsequently utilized to calculate decay rates for LFV Higgs decays (LFVHD). Within the allowed parameter space, NH contributions to LFVHD can be notably larger compared to the holomorphic counterparts. Interestingly, recently ATLAS reported an excess larger than 2σ in their searches for $h \rightarrow e\tau$ and $h \rightarrow \mu\tau$. Their best-fit point is not excluded by the corresponding CMS limits. We demonstrate that for some parts of parameter space, the predicted values for $\text{BR}(h \rightarrow e\tau)$ and $\text{BR}(h \rightarrow \mu\tau)$ in the NH scenarios reach up to the present experimental limit for these decay processes and can potentially explain the excesses observed by ATLAS, while being in agreement with other experimental constraints. If these decays are eventually observed experimentally, they could potentially serve as a distinctive signature of the NH scenarios and determine some of the NH parameters. Conversely, the limits on the LFVHDs can restrict the allowed parameter space for the NH SSB terms in the NHSSM.

*email: m.rehman@comsats.edu.pk

†email: Sven.Heinemeyer@cern.ch

1 Introduction

Neutrino oscillations [1–3] serve as a compelling indication of physics beyond the Standard Model (SM). An intriguing consequence of neutrino oscillations is the existence of lepton flavor violation (LFV), which is not explicitly allowed in the SM as the lepton flavor conservation emerges as an incidental symmetry [4]. As LFV manifests itself in the neutrino sector, there is a reasonable expectation that it may also occur in the charged lepton sector. LFV is strictly prohibited in the SM and its simple extensions predict negligible rates for charged lepton flavor violation (cLFV) decays such as $\mu \rightarrow e\gamma$, $\tau \rightarrow e\gamma$ and $\tau \rightarrow \mu\gamma$ [5, 6], rendering it beyond the reach of current experiments. Conversely, new physics models [7–9] offer the possibility of predicting cLFV at levels that can be detected by existing and future low-energy experiments. This, in turn, offers a way to constrain and assess scenarios involving new physics.

The Minimal Supersymmetric Standard Model (MSSM) [10–15] stands out as one of the most attractive and extensively studied new physics models. Beyond addressing lingering questions posed by the SM, the MSSM introduces an additional source of LFV through soft supersymmetry-breaking (SSB) terms [16, 17]. This additional degree of freedom holds the potential to yield predictions for cLFV decays at levels comparable to the existing experimental constraints on cLFV decays [18–22]. However, the conventional structure of the MSSM is increasingly constrained by the results of the Large Hadron Collider (LHC) [23], prompting researchers to explore alternatives or modifications of the MSSM. One approach involves the incorporation of nonholomorphic (NH) SSB terms [24, 25], leading to a modified model known as the nonholomorphic supersymmetric standard model (NHSSM) [26]. The additional NH terms can lead to notable phenomenological outcomes that help to align the SUSY predictions with current experimental data. As an example, the NHSSM has the potential to significantly reduce electroweak fine-tuning [27, 28]. Radiative corrections to the Higgs mass are influenced by both holomorphic and NH trilinear SSB parameters of the third generation squarks, leaving additional possibilities to more easily satisfy the Higgs-boson mass constraint [29]. Additionally, the model provides parameter space compatible with the $\text{BR}(B \rightarrow X_s + \gamma)$ constraint at high $\tan\beta$, a part of parameter space that within the MSSM without NH soft terms is more readily constrained [30].

The NHSSM has already been studied in detail [31–36], with recent attention directed towards its LFV aspects, as discussed in Ref. [37]. The latter study proposed that NH terms could potentially predict branching ratios for LFV Higgs decays (LFVHD) that are two orders of magnitude larger compared to the predictions based solely on holomorphic SSB terms. However, the analysis in Ref. [37] employed a multi-parameter scan approach, lacking a precise quantification of the specific contributions of NH terms to LFV decays. In contrast, our approach in this paper involves systematically altering one (or two) parameter(s) at a time, providing a clear indication of the NH contributions. As outlined in the following sections, this method yields predictions for LFVHD that differ from those already available in the literature. Alongside offering these refined predictions for LFVHD, we also present updated constraints on both holomorphic and NH SSB terms, originating from cLFV decays and LFVHD.

Interestingly, recently ATLAS reported an excess [38] in their searches for $h \rightarrow e\tau$ and $h \rightarrow \mu\tau$. Together these two channels show an excess larger than 2σ . Their best-fit val-

ues of $\text{BR}(h \rightarrow e\tau) \approx \text{BR}(h \rightarrow \mu\tau) \approx 0.1\%$ is not excluded by the corresponding CMS limits [39], $\text{BR}(h \rightarrow e\tau) < 0.22\%$ and $\text{BR}(h \rightarrow \mu\tau) < 0.15\%$ at the 95% C.L. limit. We demonstrate that the NHSSM can accommodate both excesses without being in conflict with other experimental limits.

For our analysis, we developed a `SPheno` [40] source code using the Mathematica package `SARAH` [41–45]. The `SARAH Scan and Plot (SSP)` [46] package served as an interface to `SPheno` for conducting numerical calculations.

The paper is organized as follows: first, we review the essential features of the NHSSM in Sect. 2. The computational framework is explained in Sect. 3 whereas the numerical results are presented in Sect. 4, including our analysis of the ATLAS excesses in their searches for $h \rightarrow e\tau$ and $h \rightarrow \mu\tau$. Finally, our conclusions can be found in Sect. 5.

2 Model set-up

The necessity for holomorphicity in the superpotential within the MSSM results in the use of holomorphic operators to parameterize the SSB sector. However, it is possible to extend the MSSM by introducing terms that violate R-Parity and/or incorporate NH terms in the SSB sector [24, 25, 47]. In its most basic formulation, the NH SSB sector of the NHSSM is given by

$$-\mathcal{L}_{\text{soft}}^{\text{NH}} = T_{ij}'^D h_2 \tilde{d}_{Ri}^* \tilde{q}_{Lj} + T_{ij}'^U h_1 \tilde{u}_{Ri}^* \tilde{q}_{Lj} + T_{ij}'^E h_2 \tilde{e}_{Ri}^* \tilde{l}_{Lj} + \mu' \tilde{h}_1 \tilde{h}_2. \quad (1)$$

Here, μ' represents the NH higgsino mass term, while $T_{ij}'^U$, $T_{ij}'^D$, and $T_{ij}'^E$ are the NH trilinear couplings associated with up-type squarks, down-type squarks, and charged sleptons, respectively. The h_1 and h_2 denote the two Higgs doublets. It is crucial to emphasize that these terms may not have a direct correlation with the holomorphic trilinear soft terms. In the presence of the NH trilinear terms, the charged slepton mass matrix can be written as,

$$M_{\tilde{L}}^2 = \begin{pmatrix} m_{\tilde{L}LL}^2 & m_{\tilde{L}LR}^2 \\ m_{\tilde{L}LR}^{2\dagger} & m_{\tilde{E}RR}^2 \end{pmatrix} \quad (2)$$

with $m_{\tilde{L}LL}^2$, $m_{\tilde{E}RR}^2$ and $m_{\tilde{L}LR}^2$ are the 3×3 matrices given by

$$\begin{aligned} m_{\tilde{L}LLij}^2 &= m_{\tilde{L}ij}^2 + M_Z^2 \cos 2\beta (I_3^L - Q_L s_W^2) \delta_{ij} + m_L^2 \delta_{ij}, \\ m_{\tilde{E}RRij}^2 &= m_{\tilde{E}ij}^2 + M_Z^2 \cos 2\beta Q_L s_W^2 \delta_{ij} + m_L^2 \delta_{ij}, \\ m_{\tilde{L}LRij}^2 &= \frac{v_1}{\sqrt{2}} \left(T_{ij}'^E - (\mu Y_{ij}'^E + T_{ij}'^E) \tan \beta \right). \end{aligned} \quad (3)$$

Here, I_3^L represents the weak isospin of leptons, Q_L stands for the electromagnetic charge, and m_L denotes the mass of the SM leptons. The subscripts L and E refer to left- and right-handed sleptons, respectively. M_Z and M_W denote the masses of the Z and W bosons, while s_W is defined as the square root of $1 - c_W^2$, where $c_W = M_W/M_Z$. Furthermore, $Y_{ij}'^E$ is the Yukawa coupling associated with leptons, the $T_{ij}'^E$ represent holomorphic trilinear couplings and $\tan \beta$ is defined as the ratio of the two vacuum expectation values of the two

Higgs doublets, denoted by v_1 and v_2 , $\tan \beta = v_2/v_1$. It should be noted that because of the different combination of fields in $\mathcal{L}_{\text{soft}}^{\text{NH}}$ w.r.t. the holomorphic SSB terms, the NH trilinear couplings $T_{ij}^{\prime E}$ receive the additional factors of $\tan \beta$ as can be seen in Eq. (3).

In addition to modifying the slepton mass matrix, the NH trilinear terms also modify the Higgs bosons coupling to charged sleptons. The couplings of the lightest Higgs boson h to charged sleptons is given by,

$$\begin{aligned}
C(h, \tilde{l}_s, \tilde{l}_t) = & -\frac{i}{4} \sum_{i,j=1}^3 \left[\left(v_1 s_\alpha + v_2 c_\alpha \right) \left(g_2^2 R_{is}^{E,*} R_{it}^E - g_1^2 \left(R_{is}^{E,*} R_{it}^E + R_{i+3,s}^{E,*} R_{i+3,t}^E \right) \right) \right. \\
& - \sum_{k=1}^3 4v_1 s_\alpha \left(R_{k+3,s}^{E,*} Y_{ik}^E Y_{ij}^E R_{j+3,t}^E - R_{js}^{E,*} Y_{ik}^E Y_{ij}^E R_{kt}^E \right) \\
& + \sqrt{2} R_{js}^{E,*} R_{i+3,t}^E \left(-2s_\alpha T_{ij}^E + c_\alpha \mu^* Y_{ij}^E + c_\alpha T_{ij}^{\prime E} \right) \\
& \left. + \sqrt{2} R_{jt}^E R_{i+3,s}^{E,*} \left(-2s_\alpha T_{ij}^E + c_\alpha T_{ij}^{\prime E} + c_\alpha \mu Y_{ij}^E \right) \right]. \tag{4}
\end{aligned}$$

Here, R_{st}^E denotes the 6×6 mixing matrix for charged sleptons, where the subscripts $s, t = 1, 2, \dots, 6$. The g_1 and g_2 stand for the gauge couplings corresponding to the $U(1)$ and $SU(2)$ gauge groups, respectively, while c_α (s_α) represent the cosine (sine) of the mixing angle α that diagonalizes the \mathcal{CP} -even Higgs sector at tree-level. Eq. (4) shows that the NH terms play a direct role in the couplings of the Higgs bosons to sfermions. This insight is particularly crucial, especially concerning Higgs decays, and can potentially result in increased decay rates compared to holomorphic terms, given that the NH terms do not directly contribute to cLFV decays but only through the charged slepton mass matrix.

3 Calculation of low-energy observables

3.1 The cLFV decays

The branching ratios for the cLFV decays such as $l_i \rightarrow l_j \gamma$, where $i, j = 1, 2, 3$ denote generations and $i > j$, can be significantly enhanced in SUSY models due to the presence of slepton flavor mixing [22, 48]. In the NHSSM, Feynman diagrams depicting cLFV decays are shown in Fig. 1. Despite having the same Feynman diagrams as in the MSSM, the presence of NH terms in the charged lepton mass matrix, as shown in Eq. (3), and the Higgs sfermion couplings, as indicated in Eq. (4), can significantly alter the contribution of each diagram. Within the NHSSM framework, diagrams involving sneutrinos ($\tilde{\nu}_i$) and charginos ($\tilde{\chi}_l$) in the loops generally have negligible impact [37]. However, those involving charged sleptons (\tilde{e}_s) and neutralinos ($\tilde{\chi}_i^0$) can be very significant, as the LFV NH terms contribute to the charged slepton mass matrix enhanced by factor of $\tan \beta$. Consequently, it is expected that the NH contributions will be dominant compared to the holomorphic ones unless T_{ij}^E is very large or if substantial cancellation occur between holomorphic and NH contributions.

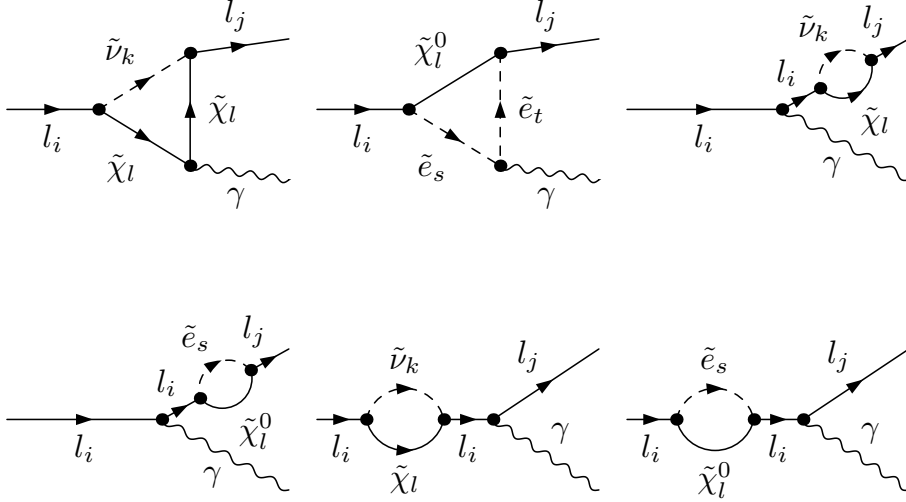


Figure 1: Feynman diagrams for the NHSSM contributions to $l_i \rightarrow l_j \gamma$ with $i, j = 1, 2, 3$ and $i > j$ (see text).

3.2 $h \rightarrow l_i l_j$ decays

The Feynman diagrams for $h \rightarrow l_i l_j$ with $i \neq j$ are shown in Fig. 2. As discussed in the preceding section, the diagrams involving sneutrinos ($\tilde{\nu}_i$) and charginos ($\tilde{\chi}_l$) remain unaffected by the NH terms for the case of LFVHD as well. However, those involving charged sleptons (\tilde{e}_s) and neutralinos ($\tilde{\chi}_i^0$) in the loop can have a significant impact. Moreover, in addition to being influenced by the LFV originating from the charged slepton mass matrix [49], the LFVHD are further affected by the presence of LFV NH terms in the coupling of the Higgs boson to charged sleptons.

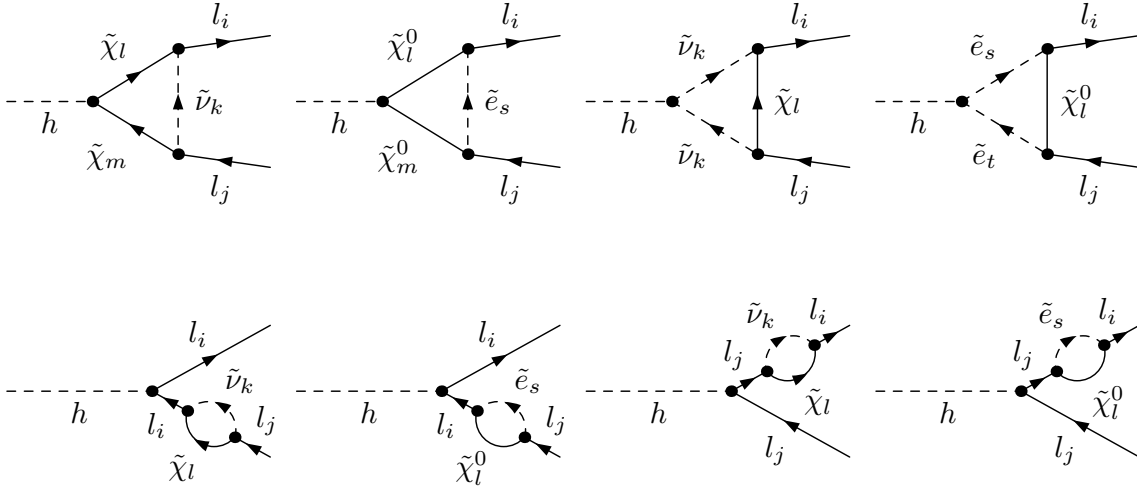


Figure 2: Feynman diagrams for the NHSSM contributions to $h \rightarrow l_i l_j$ with $i, j = 1, 2, 3$ and $i \neq j$ (see text).

3.3 Computational Setup

For our analysis, we employed the Mathematica package **SARAH** [41–45] to generate the source code for **SPheno** [40]. This source code encompasses analytical expressions pertinent to NHSSM, including mass matrices, couplings, decay rates, and branching ratios. The input parameters are provided to **SPheno** in the form of an SLHA [50] file. By utilizing this **SPheno** source code, via the corresponding SLHA output, one can obtain numerical results for mass spectra and other desired observables, such as cLFV decays and LFVHD, for any specified set of input parameters.

The **SARAH Scan and Plot (SSP)** [46] package is then employed to input parameters within a specified range. For this purpose, the **SSP** package generates an SLHA file and invokes **SPheno** within Mathematica. The output produced by **SPheno** is subsequently read by **SSP** and stored in a Mathematica-readable format. By utilizing **SSP**, one can also apply various constraints to the **SPheno**-generated output to restrict parameters to within the allowed range. We employ two types of constraints: the cLFV constraints (detailed further in Sect. 4.2) and the charge and color-breaking global minima (CCB) constraints.

It is known from the literature [51] that a substantial trilinear coupling, holomorphic or NH, generally leads to non-physical or metastable CCB minima. In the context of LFV, this concerns primarily a charge breaking vacuum, resulting from the involvement of off-diagonal entries of the trilinear couplings. The CCB constraints in the context of NHSSM were studied in detail in a Ref. [37]. To incorporate these constraints in our analysis, we developed a private Mathematica code using the expressions given in Ref. [37]. However, as we will see in the following section, the CCB constraints had little to no impact on our results.

4 Numerical Results

4.1 Input parameters

For our numerical analysis, we have selected three scenarios denoted as M_h^{125} , $M_h^{125}(\tilde{\tau})$, and $M_h^{125}(\tilde{\chi})$, originally introduced in Ref. [52]. These scenarios are parameterized in terms of electroweak-scale parameters, carefully chosen to highlight various aspects of Higgs boson phenomenology within the MSSM. It is noteworthy that these scenarios, across a broad range of their parameter space, are in agreement with the experimental findings from the LHC regarding the properties of the Higgs boson, as well as constraints on masses and couplings of new particles. Each scenario features a \mathcal{CP} -even scalar with a mass approximately around 125 GeV, exhibiting SM-like couplings (see also Ref. [53]). The first scenario, M_h^{125} , is characterized by relatively heavy superparticles, leading to Higgs phenomenology at the LHC resembling that of a Two-Higgs-Doublet Model with Higgs couplings inspired by the MSSM. On the other hand, the second and third scenarios, $M_h^{125}(\tilde{\tau})$ and $M_h^{125}(\tilde{\chi})$, involve some of the superparticles, namely staus and charginos and neutralinos respectively, being relatively light. This has implications for the decays of the heavier Higgs bosons, resulting in weakened exclusion bounds from searches involving $\tau^+\tau^-$, as well as affecting the decay of the lighter \mathcal{CP} -even scalar to photons. Importantly, these scenarios open up the possibility of exploring additional Higgs bosons through their decays to charginos and neutralinos.

Encompassing a diverse range of MSSM Higgs-boson phenomenology, the benchmark scenarios shown in Tab. 1 [52] can serve as guidelines and motivation for ongoing/upcoming LHC searches targeting additional neutral and charged Higgs bosons.

	M_h^{125}	$M_h^{125}(\tilde{\tau})$	$M_h^{125}(\tilde{\chi})$
$m_{\tilde{Q}_3}, m_{\tilde{U}_3}, m_{\tilde{D}_3}$	1500	1500	1500
$m_{\tilde{L}_3}, m_{\tilde{E}_3}$	2000	350	2000
μ	1000	1000	180
M_1	1000	180	160
M_2	1000	300	180
M_3	2500	2500	2500
X_t	2800	2800	2500
A_τ	0	800	0

Table 1: Selected scenarios in the MSSM parameter space, taken from Ref. [52]. All the dimensionful quantities are in GeV.

In Tab. 1, $m_{\tilde{Q}_3}$, $m_{\tilde{U}_3}$, and $m_{\tilde{D}_3}$ denote the third generation masses of the squark doublet, up-type squark singlet, and down-type squark singlet, respectively. Additionally, $m_{\tilde{L}_3}$ and $m_{\tilde{E}_3}$ denote the third generation masses of the left-handed slepton doublet and right-handed slepton singlet respectively. The M_1 , M_2 and M_3 are the gaugino masses and μ is the usual Higgs mixing parameter. The $X_t = A_t - \mu \cot \beta$ with $A_t = T_t/Y_t$ and $A_\tau = T_\tau/Y_\tau$ are the holomorphic trilinear couplings. In these benchmark scenarios, the SSB mass $M_{\tilde{f}}$ for the first two generations is chosen to be 2 TeV, and the holomorphic trilinear SSB terms for these generations are taken to be zero. For each scenario, we investigate four different combinations of M_A and $\tan \beta$, taking into account the latest experimental limits for MSSM Higgs-boson searches [54–56]:

$$\begin{aligned}
 \text{P1} : & M_A = 1500 \text{ GeV}, \quad \tan \beta = 7 \\
 \text{P2} : & M_A = 2000 \text{ GeV}, \quad \tan \beta = 15 \\
 \text{P3} : & M_A = 2500 \text{ GeV}, \quad \tan \beta = 30 \\
 \text{P4} : & M_A = 2500 \text{ GeV}, \quad \tan \beta = 45
 \end{aligned}$$

In the definition of the benchmark scenarios several indirect constraints such as dark matter relic density and the anomalous magnetic moment of muon were not taken into account, as their impact on parameters associated with Higgs phenomenology is minimal.

For our numerical analyses, for each scenario mentioned in Tab. 1, and for different combinations of M_A and $\tan \beta$ as specified above, we vary one off-diagonal entry of either T_{ij}^E or $T_{ij}'^E$ within the range of $(-10000 : 10000)$ GeV, while setting all other off-diagonal entries to zero. Subsequently, we only consider those values of T_{ij}^E and $T_{ij}'^E$ that comply with the constraints imposed by cLFV decays, in order to obtain predictions for LFVHD. Here, we indicate the regions of parameter space that are already probed by the ATLAS and CMS experiments, particularly for $h \rightarrow e\tau$ and $h \rightarrow \mu\tau$.

4.2 cLFV Constraints

Decays involving cLFV, such as $l_i \rightarrow l_j \gamma$, where l_i represents a charged lepton with the generation index $i, j = 1, 2, 3$ and $i > j$, impose the most rigorous constraints on LFV due to exceptionally tight limits on these decay processes. Notably, the upper limits on the processes involving $\mu - e$ transition such as $\mu \rightarrow e \gamma$ and conversion rate $\text{CR}(\mu - e, \text{Au})$, are particularly stringent, significantly constraining LFV within the $\mu - e$ sector. In contrast, the constraints on transitions involving $\tau - e$ and $\tau - \mu$ are comparatively weaker, allowing for considerable LFV that can be explored in present experiments.

In Tab. 2, we list the present constraints on cLFV [57] and LFVHD decays. Concerning the latter, the limits on decays involving taus are based on Ref. [39] (later labeled as ‘‘CMS’’), whereas the $h \rightarrow e\mu$ limit is taken from Ref. [58].

Process	Limit	Process	Limit
$\text{BR}(\mu \rightarrow e\gamma)$	4.2×10^{-13}	$\text{BR}(\mu \rightarrow 3e)$	1.0×10^{-12}
$\text{CR}(\mu - e, \text{Au})$	7.0×10^{-13}	$\text{CR}(\mu - e, \text{Ti})$	4.3×10^{-13}
$\text{BR}(\tau \rightarrow e\gamma)$	3.3×10^{-8}	$\text{BR}(\tau \rightarrow 3e)$	2.7×10^{-8}
$\text{BR}(\tau \rightarrow \mu\gamma)$	4.4×10^{-8}	$\text{BR}(\tau \rightarrow 3\mu)$	2.1×10^{-8}
$\text{BR}(h \rightarrow e\mu)$	6.1×10^{-5}	$\text{BR}(h \rightarrow e\tau)$	2.2×10^{-3}
$\text{BR}(h \rightarrow \mu\tau)$	1.5×10^{-3}		

Table 2: Present upper bounds on the cLFV decays and LFV Higgs decays [39, 57, 58] (see text). The bounds on LFVHD involving taus are indicated in the plots where applicable (labeled as ‘‘CMS’’).

The limits presented in Tab. 2 impose stringent constraints on the LFV holomorphic and NH SSB terms. By utilizing the input parameters provided in Tab. 1, we have computed the allowed range for T_{ij}^E and $T'_{ij}{}^E$. It is assumed that only one of the couplings T_{ij}^E or $T'_{ij}{}^E$ is non-zero at a given time, where $T_{ij} = Y_{ij} A_{ij}$ and $T'_{ij} = Y_{ij} A'_{ij}$. A non-zero value of either T_{ij}^E or $T'_{ij}{}^E$ will result in a non-zero value of Y_{ij}^E . In Tab. 3, we show the constraints on T_{ij}^E and $T'_{ij}{}^E$ in the M_h^{125} , $M_h^{125}(\tilde{\tau})$, and $M_h^{125}(\tilde{\chi})$ scenarios.

As evident from Tab. 3, the couplings T_{ij}^E and $T'_{ij}{}^E$ involving the $\mu - e$ transition stand out as the most constrained. This can be primarily attributed to the strong experimental constraints on $\text{BR}(\mu \rightarrow e\gamma)$. In contrast, the couplings related to $\tau - e$ or $\tau - \mu$ transitions can be larger by $\mathcal{O}(10^3)$, mainly due to the comparatively weaker experimental constraints on $\text{BR}(\tau \rightarrow e\gamma)$ and $\text{BR}(\tau \rightarrow \mu\gamma)$, which are of $\mathcal{O}(10^{-8})$. Despite the fact that cLFV decays are the primary constraining factor, certain values of T_{ij}^E and $T'_{ij}{}^E$ are excluded because they lead to negative scalar lepton masses. For instance, the point P4, where $\tan\beta = 45$ in the $M_h^{125}(\tilde{\tau})$ scenario, results in negative scalar lepton masses and is thus excluded.

M_h^{125}												
	$ T_{12}^E $	$ T_{12}'^E $	$ T_{21}^E $	$ T_{21}'^E $	T_{13}^E	$ T_{13}'^E $	$ T_{31}^E $	$ T_{31}'^E $	$ T_{23}^E $	$ T_{23}'^E $	$ T_{32}^E $	$ T_{32}'^E $
$P1$	0.946	0.135	0.946	0.135	4855	1486	5108	1432	5108	1702	5324	1630
$P2$	2.027	0.135	2.027	0.135	5972	1486	6441	1432	6153	1684	6549	1630
$P3$	4.099	0.135	4.099	0.135	6549	1468	7095	1414	6675	1684	7095	1612
$P4$	6.189	0.135	6.189	0.135	6747	1468	7109	1396	6855	1666	7109	1612
$M_h^{125}(\tilde{\tau})$												
	$ T_{12}^E $	$ T_{12}'^E $	$ T_{21}^E $	$ T_{21}'^E $	T_{13}^E	$ T_{13}'^E $	$ T_{31}^E $	$ T_{31}'^E $	$ T_{23}^E $	$ T_{23}'^E $	$ T_{32}^E $	$ T_{32}'^E $
$P1$	2.460	0.375	2.460	0.375	1006	198.0	909.0	209.0	1096	228.0	963.0	240.0
$P2$	5.270	0.373	5.270	0.375	1406	187.0	1180	208.0	1468	215.0	1216	239.0
$P3$	10.54	0.373	10.59	0.373	1396	149.0	1085	169.0	1414	172.0	1085	194.0
$M_h^{125}(\tilde{\chi})$												
	$ T_{12}^E $	$ T_{12}'^E $	$ T_{21}^E $	$ T_{21}'^E $	T_{13}^E	$ T_{13}'^E $	$ T_{31}^E $	$ T_{31}'^E $	$ T_{23}^E $	$ T_{23}'^E $	$ T_{32}^E $	$ T_{32}'^E $
$P1$	2.710	0.405	2.710	0.405	4846	3234	6135	3108	5972	3504	6225	3378
$P2$	5.790	0.405	5.790	0.405	6405	3216	6783	3108	6477	3486	6801	3378
$P3$	11.62	0.405	11.62	0.405	6657	3216	4261	3072	6729	3486	4747	3342
$P4$	17.74	0.405	17.56	0.405	6783	3216	2972	3036	6837	3468	3432	3306

Table 3: Upper limits on T_{ij}^E and $T_{ij}'^E$ arising from cLFV decays within the M_h^{125} , $M_h^{125}(\tilde{\tau})$ and $M_h^{125}(\tilde{\chi})$ scenarios. All the dimensionful quantities are in GeV.

4.3 $h \rightarrow l_i l_j$ decays

The large values of both holomorphic and NH trilinear couplings in the $\tau - e$ and $\tau - \mu$ sectors can result in large branching ratios for LFVHD. Specifically, the NH terms can have non-negligible effects on Higgs phenomenology, as these terms directly contribute to the Higgs coupling with the sleptons.

For LFV Higgs decays, our findings are illustrated in Figs. 3-7. Fig. 3 displays the $\text{BR}(h \rightarrow e\mu)$ as a function of T_{12}^E (left column) and $T_{12}'^E$ (right column) in the scenarios M_h^{125} (upper row), $M_h^{125}(\tilde{\tau})$ (middle row), and $M_h^{125}(\tilde{\chi})$ (lower row). The plots show that $\text{BR}(h \rightarrow e\mu)$ can reach values of the $\mathcal{O}(10^{-17})$ ($\mathcal{O}(10^{-10})$) for T_{12}^E ($T_{12}'^E$) in M_h^{125} scenario while in $M_h^{125}(\tilde{\tau})$ they are one-order-of-magnitude smaller compared to M_h^{125} scenario. In the $M_h^{125}(\tilde{\chi})$ scenario, the $\text{BR}(h \rightarrow e\mu)$ remain around $\mathcal{O}(10^{-17})$ ($\mathcal{O}(10^{-18})$) for T_{12}^E ($T_{12}'^E$). Interestingly, despite being more constrained compared to T_{12}^E , the coupling $T_{12}'^E$ can result in a branching ratio for $h \rightarrow e\mu$ that is seven orders of magnitude larger compared to the T_{12}^E contributions in M_h^{125} and $M_h^{125}(\tilde{\tau})$ scenarios while still adhering to the constraints on cLFV decays. However, the obtained values are far below the current or anticipated future limits (see below). As anticipated, the $T_{12}'^E$ contributions increase with increasing values of $\tan\beta$ and the most substantial contributions are observed for the point P4, where $\tan\beta = 45$, which can be attributed to the multiplication of NH $T_{ij}'^E$ couplings by $\tan\beta$. The results for $\text{BR}(h \rightarrow e\mu)$ as a function of T_{21}^E ($T_{21}'^E$) exhibit similar trends to those for T_{12}^E ($T_{12}'^E$), and are

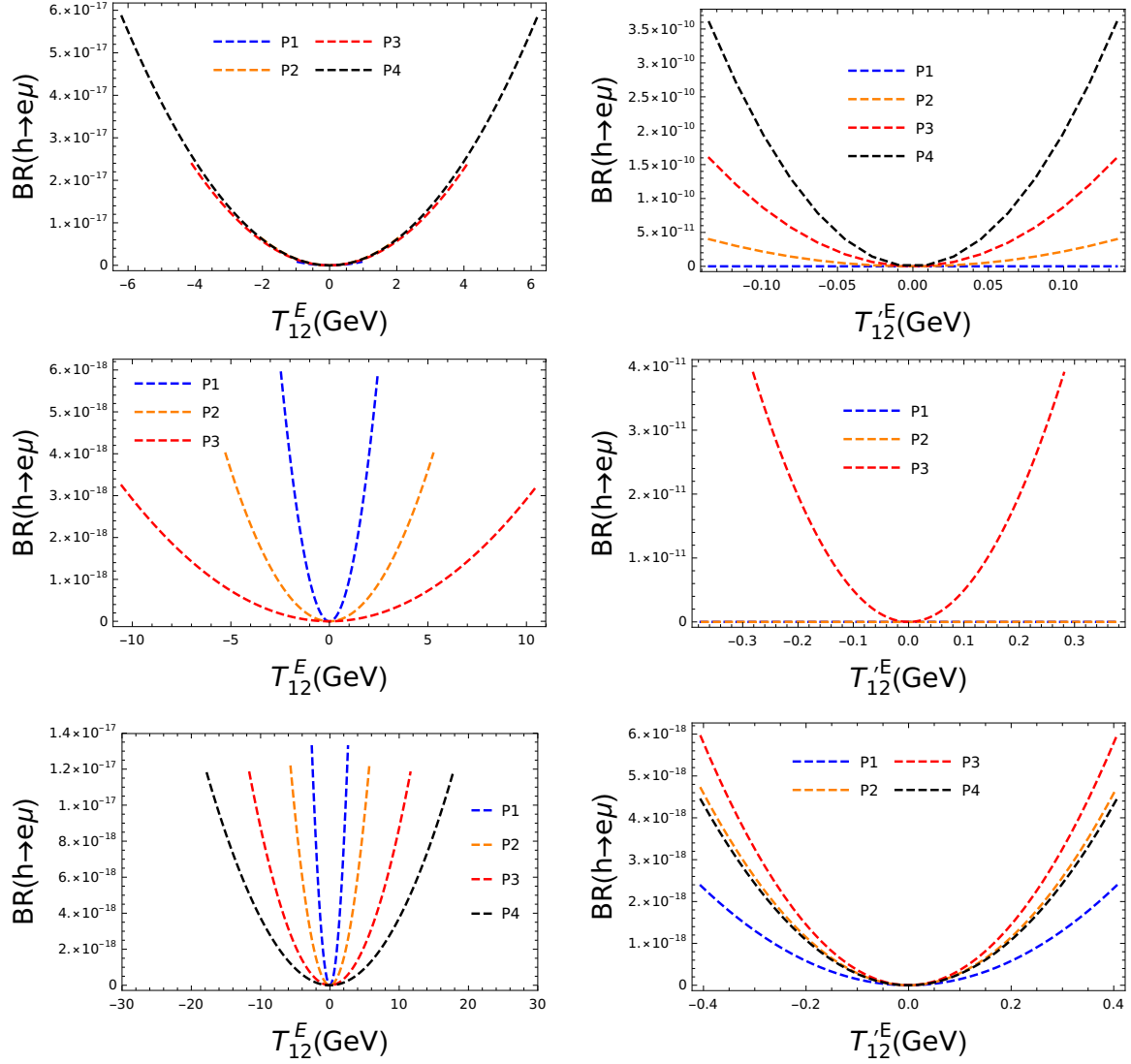


Figure 3: $\text{BR}(h \rightarrow e\mu)$ as a function of T_{12}^E (left column) and $T_{12}'^E$ (right column) within the M_h^{125} (upper row), $M_h^{125}(\tilde{\tau})$ (middle row) and $M_h^{125}(\tilde{\chi})$ (lower row) scenarios.

not presented here.

Fig. 4 illustrates the $\text{BR}(h \rightarrow e\tau)$ as a function of T_{13}^E and $T_{13}'^E$. The arrangement of plots is same as in the previous figure. In the context of M_h^{125} , the $\text{BR}(h \rightarrow e\tau)$ can be three-order-of-magnitude larger for $T_{13}'^E$, reaching up to $\mathcal{O}(10^{-2})$, compared to T_{13}^E , where it can only reach up to $\mathcal{O}(10^{-5})$. In the upper right plot we have indicated the bounds on $T_{13}'^E$ that are placed by the current limits on $\text{BR}(h \rightarrow e\tau)$, see Tab. 2. In the context of the $M_h^{125}(\tilde{\tau})$ scenario, for points P3, the contributions of T_{13}^E to $\text{BR}(h \rightarrow e\tau)$ are found at levels around $\mathcal{O}(10^{-9})$. Conversely, for P1 and P2, these contributions are even smaller. In contrast, contributions from $T_{13}'^E$ reach around $\mathcal{O}(10^{-4})$ for P3, while maintaining values of approximately $\mathcal{O}(10^{-10})$ and $\mathcal{O}(10^{-9})$ for P1 and P2, respectively. For the $M_h^{125}(\tilde{\chi})$ scenario, $T_{13}'^E$ contributions can be two orders of magnitude larger than T_{13}^E contributions for P3, while only a one-order-of-magnitude difference is observed for other points. Fig. 5 depicts

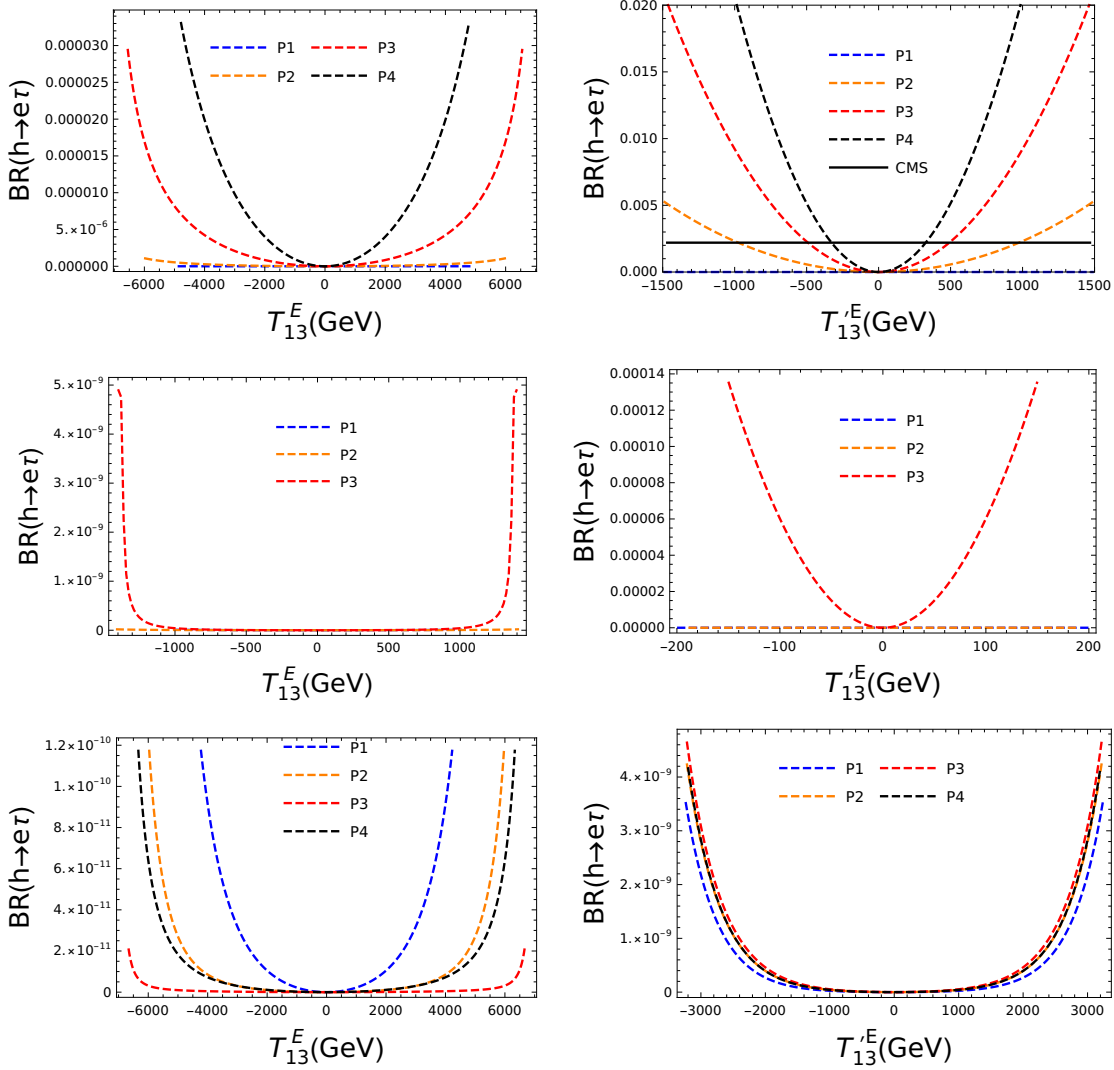


Figure 4: $\text{BR}(h \rightarrow e\tau)$ as a function of T_{13}^E (left column) and $T'_{13}{}^E$ (right column) within the M_h^{125} (upper row), $M_h^{125}(\tilde{\tau})$ (middle row) and $M_h^{125}(\tilde{\chi})$ (lower row) scenarios. The horizontal solid line in the upper right plot indicates the experimental limit, see Tab. 2.

the dependence of $\text{BR}(h \rightarrow e\tau)$ on T_{31}^E and $T'_{31}{}^E$. The arrangement of the plots follows the same pattern as in previous figures. Once again, in the M_h^{125} and $M_h^{125}(\tilde{\tau})$ scenarios, the $T'_{31}{}^E$ coupling can yield significantly large contributions compared to T_{31}^E , even though the allowed range for $T'_{31}{}^E$ is considerably smaller than that of T_{31}^E . For the points P3 and P4, the $\text{BR}(h \rightarrow e\tau)$ can attain values up to $\mathcal{O}(10^{-2})$ in M_h^{125} scenario. As in Fig. 4 we have indicated in the upper right plot the limits placed on $T'_{31}{}^E$ from the existing limits on $\text{BR}(h \rightarrow e\tau)$, see Tab. 2. In the $M_h^{125}(\tilde{\chi})$ scenario, the results exhibit nearly identical patterns, with $T'_{31}{}^E$ resulting in a branching ratio approximately one order of magnitude larger than that predicted by T_{31}^E .

The $\text{BR}(h \rightarrow \mu\tau)$ as a function of T_{23}^E and $T'_{23}{}^E$ is shown in Fig. 6. Again, the arrangement of the plots is same as in the previous figures. The NH trilinear coupling's effects are more pronounced in M_h^{125} and $M_h^{125}(\tilde{\tau})$ and less significant for $M_h^{125}(\tilde{\chi})$ as was observed in

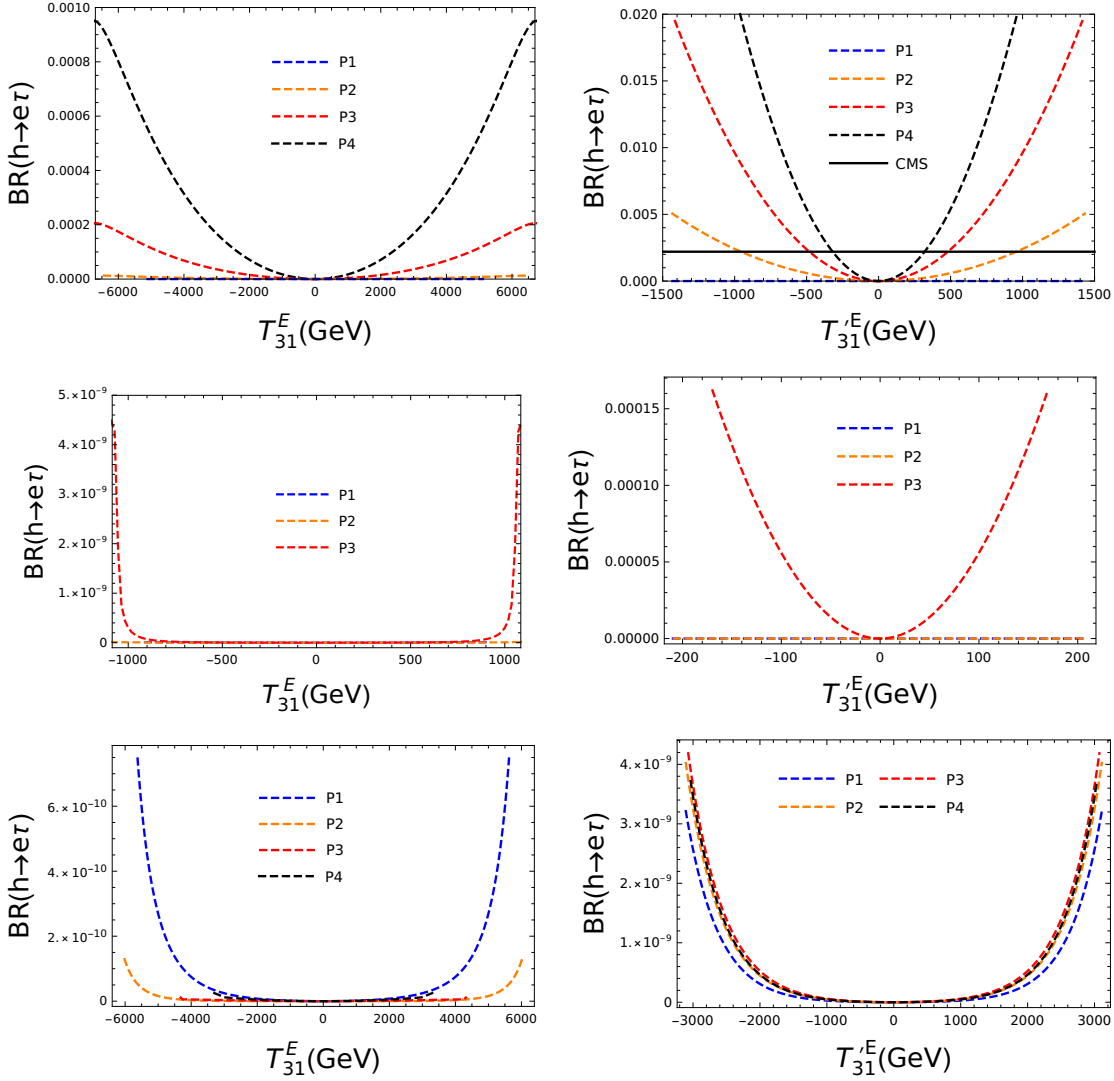


Figure 5: $\text{BR}(h \rightarrow e\tau)$ as a function of T_{31}^E (left column) and $T_{31}'^E$ (right column) within the M_h^{125} (upper row), $M_h^{125}(\tilde{\tau})$ (middle row) and $M_h^{125}(\tilde{\chi})$ (lower row) scenarios. The horizontal solid line in the upper right plot indicates the experimental limit, see Tab. 2.

previous figures. As before, in the M_h^{125} scenario the parameter space of $T_{23}'^E$ is restricted now from $\text{BR}(h \rightarrow \mu\tau)$ as indicated in the upper right plot. The relative difference between contributions from T_{23}^E and $T_{23}'^E$ mirrors that of T_{13}^E and $T_{13}'^E$. Finally, we present the dependence of $\text{BR}(h \rightarrow \mu\tau)$ on T_{32}^E and $T_{32}'^E$ in Fig. 7. These plots exhibit a similar pattern to the one discussed earlier in relation to Fig. 5. Again, in the M_h^{125} scenario bounds on $T_{32}'^E$ are placed by the current bounds on $\text{BR}(h \rightarrow \mu\tau)$. All the bounds on NH parameters found in this scenario from the existing limits on $\text{BR}(h \rightarrow e\tau)$ and $\text{BR}(h \rightarrow \mu\tau)$ are summarized in Tab. 4. The limits from cLFV are given for comparison and are identical to Tab. 3.

Finally, for completeness, in Tab. 5, we provide future experimental bounds on cLFV and LFVHDs. These bounds are smaller by $\mathcal{O}(10^{-1})$ compared to the current experimental bounds. Concerning the future anticipated bounds cLFV decays, in case of no discovery, they will restrict severely the allowed parameter space of the NH SSB terms. Concerning the

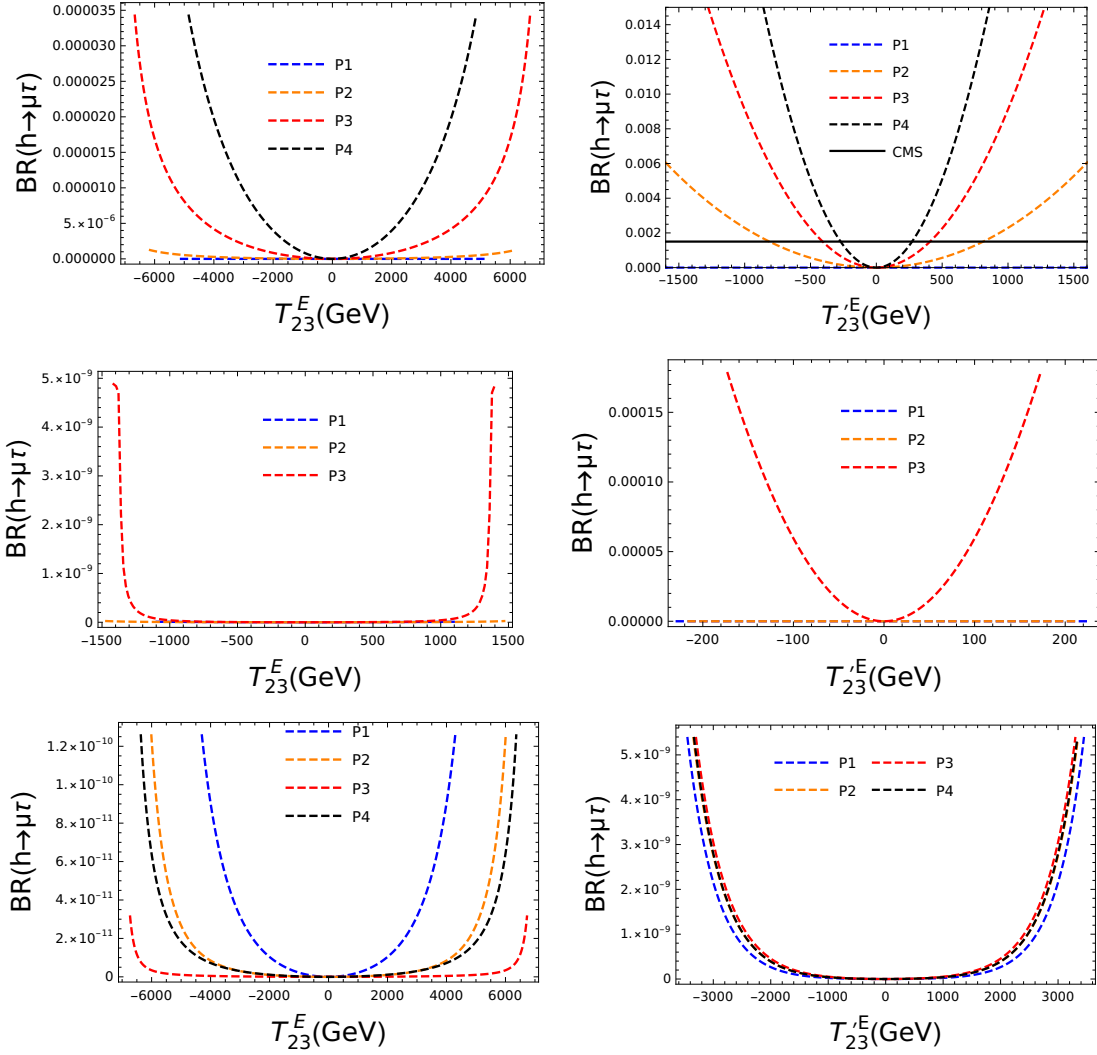


Figure 6: $\text{BR}(h \rightarrow \mu\tau)$ as a function of T_{23}^E (left column) and $T_{23}'^E$ (right column) within the M_h^{125} (upper row), $M_h^{125}(\tilde{\tau})$ (middle row) and $M_h^{125}(\tilde{\chi})$ (lower row) scenarios. The horizontal solid line in the upper right plot indicates the experimental limit, see Tab. 2.

future sensitivities on LFVHVs, it becomes clear that the excesses observed by ATLAS, see also the next subsection, can conclusively be tested. In particular in the M_h^{125} scenario these bounds can restrict severely the allowed parameter space of some of the NH SSB parameters.

In summary, NH trilinear couplings can yield significantly larger contributions compared to holomorphic contributions, particularly in M_h^{125} and $M_h^{125}(\tilde{\tau})$. For $M_h^{125}(\tilde{\chi})$, the predictions are small because μ is smaller ($\mu = 180$ GeV) compared to M_h^{125} or $M_h^{125}(\tilde{\tau})$, where $\mu = 1000$ GeV. The parameter μ appears in the mass matrix and in the couplings multiplied by Y_{ij}^E . The non-zero values of T_{ij}^E or $T_{ij}'^E$ correspond to a non-zero Y_{ij}^E , which appears as a prefactor of μ in the mass matrices and couplings. Consequently, a larger μ will lead to larger LFV contributions.

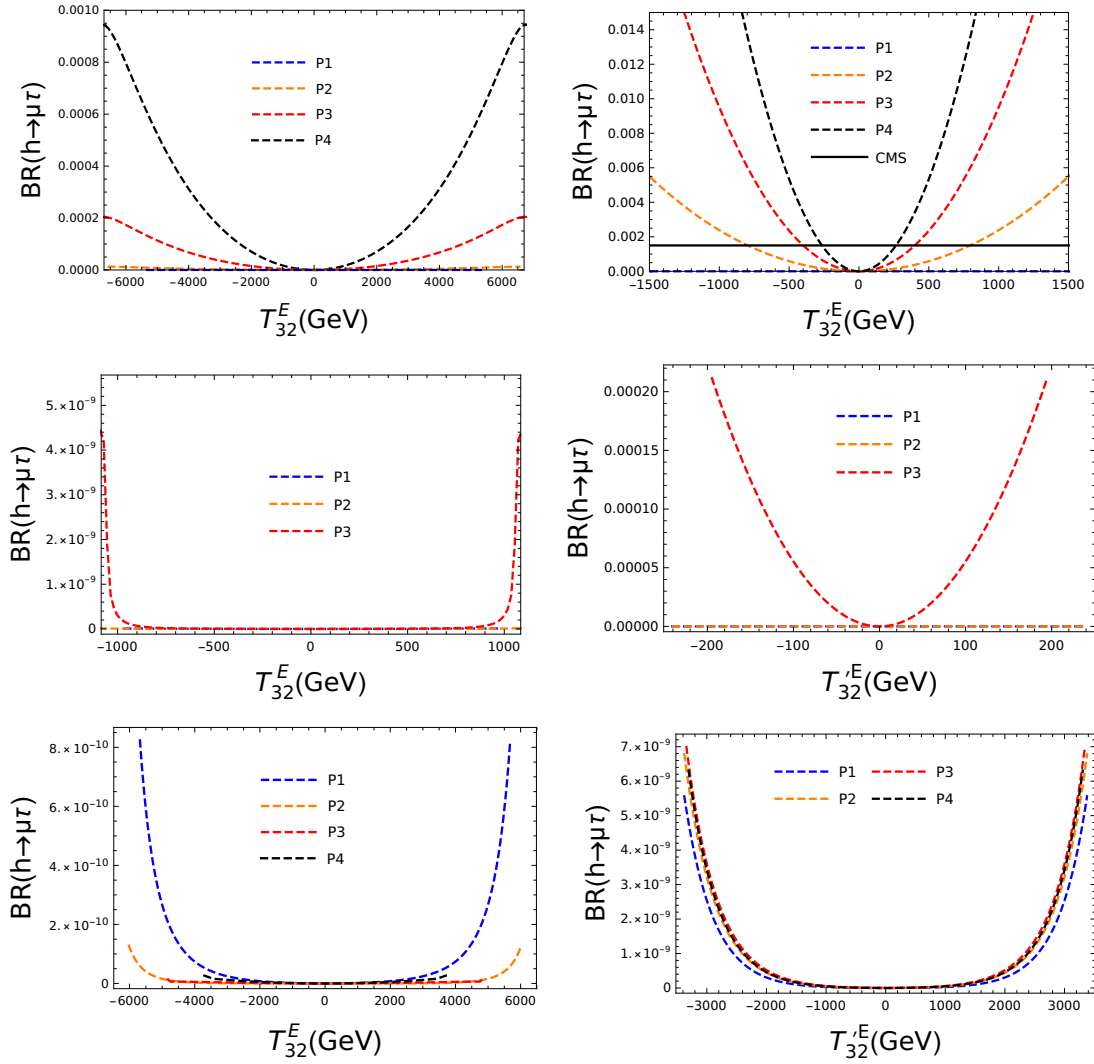


Figure 7: $\text{BR}(h \rightarrow \mu\tau)$ as a function of T_{32}^E (left column) and $T_{32}'^E$ (right column) within the M_h^{125} (upper row), $M_h^{125}(\tilde{\tau})$ (middle row) and $M_h^{125}(\tilde{\chi})$ (lower row) scenarios. The horizontal solid line in the upper right plot indicates the experimental limit, see Tab. 2.

	P2		P3		P4	
	cLFV	LFVHD	cLFV	LFVHD	cLFV	LFVHD
$ T_{13}'^E $	1486	963	1468	477	1468	315
$ T_{31}'^E $	1432	945	1414	477	1396	315
$ T_{23}'^E $	1684	801	1684	405	1666	261
$ T_{32}'^E $	1612	783	1612	387	1612	261

Table 4: Constraints on $T_{ij}'^E$ arising from LFV Higgs decays within the M_h^{125} scenario. All the dimensionful quantities are in GeV. The limits from cLFV are given for comparison and are identical to Tab. 3

cLFV Decays	Limit	LFVHD	Limit
$\text{BR}(\mu \rightarrow e\gamma)$	6.0×10^{-14} [59]	$\text{BR}(h \rightarrow e\mu)$	1.2×10^{-5} [60]
$\text{BR}(\tau \rightarrow e\gamma)$	9.0×10^{-9} [61]	$\text{BR}(h \rightarrow e\tau)$	1.6×10^{-4} [60]
$\text{BR}(\tau \rightarrow \mu\gamma)$	6.9×10^{-9} [61]	$\text{BR}(h \rightarrow \mu\tau)$	1.4×10^{-4} [60]

Table 5: Future upper bounds on the cLFV decays and LFV Higgs decays [59–61].

4.4 The ATLAS excess

Recently ATLAS reported an excess [38] in their searches for $h \rightarrow e\tau$ and $h \rightarrow \mu\tau$. Together these two channels show an excess larger than 2σ . Their best-fit values of $\text{BR}(h \rightarrow e\tau) \approx \text{BR}(h \rightarrow \mu\tau) \approx 0.1\%$ is not excluded by the corresponding CMS limits [39], $\text{BR}(h \rightarrow e\tau) < 0.22\%$ and $\text{BR}(h \rightarrow \mu\tau) < 0.15\%$ at the 95% C.L. limit. In the previous subsection we have demonstrated that the NHSSM can yield values of these two BRs that are in the ballpark of the ATLAS excess for each of the two BRs individually. In this section we demonstrate that the NHSSM can accommodate both excesses simultaneously without being in conflict with other experimental limits.

In the upper plots of Fig. 8 we show the $\text{BR}(h \rightarrow \mu\tau)$ – $\text{BR}(h \rightarrow e\tau)$ plane indicating the ATLAS excess (ellipses) and the CMS bounds (horizontal and vertical solid lines). The red stars denote the best-fit point from ATLAS [38]. Within the M_h^{125} scenario for P4 (i.e. $M_A = 2500$ GeV, $\tan\beta = 45$), we randomly scanned $T'_{13}{}^E$ ($T'_{31}{}^E$) and $T'_{23}{}^E$ ($T'_{32}{}^E$), yielding the upper left (right) plot. For all points we took into account the current bounds from cLFV. One can observe that the 1σ ellipse of the ATLAS excesses is well populated for the scan varying $T'_{13}{}^E$ and $T'_{23}{}^E$ (upper left plot), while only the “lower values” of the ellipse are populated in the scan of $T'_{31}{}^E$ and $T'_{32}{}^E$ (upper right plot).

In the lower row of Fig. 8 we show the points found in the 1σ and 2σ ellipses in the upper row as green and yellow points, respectively, in the $T'_{13}{}^E$ – $T'_{23}{}^E$ plane (left plot) and in the $T'_{31}{}^E$ – $T'_{32}{}^E$ plane (right plot). All points are below the respective CMS limits indicated as solid horizontal and vertical lines in the upper plots. One can observe that the NH contribution to $\text{BR}(h \rightarrow \mu\tau)$ and $\text{BR}(h \rightarrow e\tau)$ are invariant under the signs of $T'_{ij}{}^E$. The points inside the 1σ ellipses are found for $100 \text{ GeV} \lesssim |T'_{13,31}{}^E| \lesssim 250 \text{ GeV}$ and $180 \text{ GeV} \lesssim |T'_{23,32}{}^E| \lesssim 280 \text{ GeV}$.

Overall, we conclude that the NHSSM can describe the observed excesses well, while being in agreement with the existing experimental bounds.

5 Conclusions

The MSSM including nonholomorphic soft SUSY-breaking terms (NHSSM) is a well motivated model going beyond the SM and extending non-trivially the MSSM. Within the NHSSM, we investigated the effects of lepton flavor violating terms. In a first step we applied the current bounds from charged lepton flavor violating (cLFV) decays, $l_i \rightarrow l_j\gamma$ ($i, j = 1, 2, 3$, $i > j$, $l_{1,2,3} = e, \mu, \tau$) to set limits on the NH flavor violating soft SUSY-breaking parameters, $T'_{ij}{}^E$ ($i, j = 1, 2, 3$). Our approach, systematically altering one parameter at a time, provides a clear indication of the NH contributions to the cLFV decays.

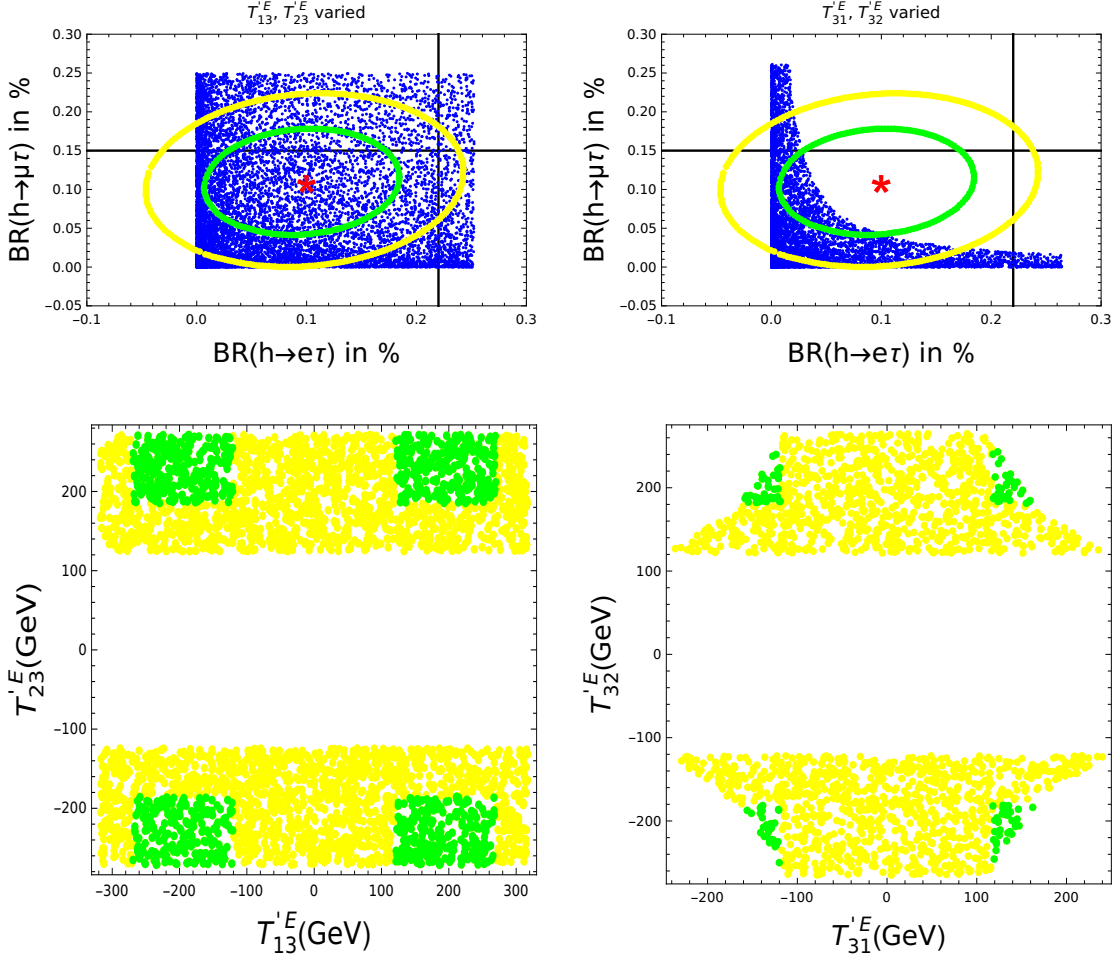


Figure 8: Upper row: the $\text{BR}(h \rightarrow \mu\tau)$ – $\text{BR}(h \rightarrow e\tau)$ plane showing the ATLAS excess (ellipses), the CMS bounds (horizontal and vertical solid lines), and our predictions in the M_h^{125} scenario for P4 ($M_A = 2500$ GeV, $\tan\beta = 45$) with both T'_{13} and T'_{23} varied independently (upper-left plot) and T'_{31} and T'_{32} (upper-right plot). Lower row: the points found in the 1σ and 2σ ellipses of the ATLAS excesses are shown in the T'_{13} – T'_{23} (lower-left) and T'_{31} – T'_{32} (lower-right) plane as yellow and green dots, respectively.

In a second step we calculated LFV Higgs decays (LFVHD), $h \rightarrow l_i l_j$ ($i, j = 1, 2, 3$, $i \neq j$), taking into account the bounds on T'_{ij} obtained from cLFV decays. We found that the $\text{BR}(h \rightarrow l_i l_j)$ can reach values far above the corresponding SM values (as was known from the literature), but even reaching and exceeding the current bounds from CMS and ATLAS.

Interestingly, recently ATLAS reported an excess [38] in their searches for $h \rightarrow e\tau$ and $h \rightarrow \mu\tau$. Together these two channels show an excess larger than 2σ . Their best-fit values of $\text{BR}(h \rightarrow e\tau) \approx \text{BR}(h \rightarrow \mu\tau) \approx 0.1\%$ is not excluded by the corresponding CMS limits [39], $\text{BR}(h \rightarrow e\tau) < 0.22\%$ and $\text{BR}(h \rightarrow \mu\tau) < 0.15\%$ at the 95% C.L. limit. We varied independently the parameters T'_{13} , T'_{23} or T'_{31} , T'_{32} to test whether the ATLAS excess can be described within the NHSSM. We demonstrate that the model can accommodate both excesses without being in conflict with other experimental limits. If these decays are

eventually observed experimentally, they could potentially serve as a distinctive signature of the NH scenarios and determine some of the NH parameters. Conversely, the limits on the LFVHDs can restrict the allowed parameter space for the NH SSB terms in the NHSSM.

Acknowledgments

The work of M.R. was supported by HEC Pakistan, under NRPB grant 20-15867/NRPB/R&D/HEC/2021. The work of S.H. has received financial support from the PID2022-142545NB-C21 funded by MCIN/AEI/10.13039/501100011033/ FEDER, UE and in part by the grant IFT Centro de Excelencia Severo Ochoa CEX2020-001007-S funded by MCIN/AEI/10.13039/501100011033.

References

- [1] Y. Fukuda *et al.* [Super-Kamiokande], Phys. Rev. Lett. **81** (1998), 1562-1567 [arXiv:hep-ex/9807003 [hep-ex]].
- [2] Q. R. Ahmad *et al.* [SNO], Phys. Rev. Lett. **87** (2001), 071301 [arXiv:nucl-ex/0106015 [nucl-ex]].
- [3] Q. R. Ahmad *et al.* [SNO], Phys. Rev. Lett. **89** (2002), 011301 [arXiv:nucl-ex/0204008 [nucl-ex]].
- [4] G. Isidori, J. Pagès and F. Wilsch, JHEP **03** (2022), 011 [arXiv:2111.13724 [hep-ph]].
- [5] W. J. Marciano and A. I. Sanda, Phys. Lett. B **67** (1977), 303-305
- [6] T. P. Cheng and L. F. Li, Phys. Rev. Lett. **45** (1980), 1908
- [7] J. Hisano, T. Moroi, K. Tobe, M. Yamaguchi and T. Yanagida, Phys. Lett. B **357** (1995), 579-587 [arXiv:hep-ph/9501407 [hep-ph]].
- [8] J. R. Ellis, J. Hisano, M. Raidal and Y. Shimizu, Phys. Rev. D **66** (2002), 115013 [arXiv:hep-ph/0206110 [hep-ph]].
- [9] M. Sher, Phys. Rev. D **66** (2002), 057301 [arXiv:hep-ph/0207136 [hep-ph]].
- [10] P. Fayet, Nucl. Phys. B **90** (1975), 104-124
- [11] P. Fayet, Phys. Lett. B **64** (1976), 159
- [12] P. Fayet, Phys. Lett. B **69** (1977), 489
- [13] H. P. Nilles, Phys. Rept. **110** (1984), 1-162
- [14] H. E. Haber and G. L. Kane, Phys. Rept. **117** (1985), 75-263
- [15] R. Barbieri, Riv. Nuovo Cim. **11N4** (1988), 1-45

- [16] L. J. Hall, V. A. Kostelecky and S. Raby, Nucl. Phys. B **267** (1986), 415-432
- [17] F. Borzumati and A. Masiero, Phys. Rev. Lett. **57** (1986), 961
- [18] I. Masina and C. A. Savoy, Nucl. Phys. B **661** (2003), 365-393 [arXiv:hep-ph/0211283 [hep-ph]].
- [19] P. Paradisi, JHEP **10** (2005), 006 [arXiv:hep-ph/0505046 [hep-ph]].
- [20] A. Crivellin, Phys. Rev. D **83** (2011), 056001 [arXiv:1012.4840 [hep-ph]].
- [21] A. Crivellin, L. Hofer and J. Rosiek, JHEP **07** (2011), 017 [arXiv:1103.4272 [hep-ph]].
- [22] M. Arana-Catania, S. Heinemeyer and M. J. Herrero, Phys. Rev. D **88** (2013) no.1, 015026 [arXiv:1304.2783 [hep-ph]].
- [23] S. Sekmen [ATLAS, CMS and LHCb], [arXiv:2204.03053 [hep-ex]].
- [24] L. Girardello and M. T. Grisaru, Nucl. Phys. B **194** (1982), 65
- [25] J. Bagger and E. Poppitz, Phys. Rev. Lett. **71** (1993), 2380-2382 [arXiv:hep-ph/9307317 [hep-ph]].
- [26] M. Cakir, S. Mutlu and L. Solmaz, Phys. Rev. D **71** (2005), 115005 [arXiv:hep-ph/0501286 [hep-ph]].
- [27] G. G. Ross, K. Schmidt-Hoberg and F. Staub, Phys. Lett. B **759** (2016), 110-114 [arXiv:1603.09347 [hep-ph]].
- [28] G. G. Ross, K. Schmidt-Hoberg and F. Staub, JHEP **03** (2017), 021 [arXiv:1701.03480 [hep-ph]].
- [29] M. Rehman and S. Heinemeyer, Phys. Rev. D **107** (2023) no.9, 095033 [arXiv:2212.13757 [hep-ph]].
- [30] U. Chattopadhyay and A. Dey, JHEP **10** (2016), 027 doi:10.1007/JHEP10(2016)027 [arXiv:1604.06367 [hep-ph]].
- [31] C. S. Un, S. H. Tanyıldızı, S. Kerman and L. Solmaz, Phys. Rev. D **91** (2015) no.10, 105033 [arXiv:1412.1440 [hep-ph]].
- [32] I. Jack and D. Jones, Phys. Lett. B **457** (1999), 101-108 [arXiv:hep-ph/9903365 [hep-ph]].
- [33] I. Jack and D. Jones, Phys. Rev. D **61** (2000), 095002 [arXiv:hep-ph/9909570 [hep-ph]].
- [34] I. Jack, D. Jones and A. Kord, Phys. Lett. B **588** (2004), 127-135 [arXiv:hep-ph/0402045 [hep-ph]].
- [35] A. Sabanci, A. Hayreter and L. Solmaz, Phys. Lett. B **661** (2008), 154-157 [arXiv:0801.2029 [hep-ph]].

- [36] S. Israr and M. Rehman, [arXiv:2407.01210 [hep-ph]].
- [37] U. Chattopadhyay, D. Das and S. Mukherjee, JHEP **06** (2020), 015 [arXiv:1911.05543 [hep-ph]].
- [38] G. Aad *et al.* [ATLAS], JHEP **07** (2023), 166 [arXiv:2302.05225 [hep-ex]].
- [39] A. M. Sirunyan *et al.* [CMS], Phys. Rev. D **104** (2021) no.3, 032013 [arXiv:2105.03007 [hep-ex]].
- [40] W. Porod, Comput. Phys. Commun. **153** (2003), 275-315 [arXiv:hep-ph/0301101 [hep-ph]].
- [41] F. Staub, Comput. Phys. Commun. **181** (2010), 1077-1086 [arXiv:0909.2863 [hep-ph]].
- [42] F. Staub, Comput. Phys. Commun. **182** (2011), 808-833 [arXiv:1002.0840 [hep-ph]].
- [43] F. Staub, Comput. Phys. Commun. **184** (2013), 1792-1809 [arXiv:1207.0906 [hep-ph]].
- [44] F. Staub, Comput. Phys. Commun. **185**, 1773 (2014) [arXiv:1309.7223 [hep-ph]].
- [45] F. Staub, Adv. High Energy Phys. **2015** (2015), 840780 [arXiv:1503.04200 [hep-ph]].
- [46] F. Staub, T. Ohl, W. Porod and C. Speckner, Comput. Phys. Commun. **183** (2012), 2165-2206 [arXiv:1109.5147 [hep-ph]].
- [47] J. Chakraborty and S. Roy, Phys. Rev. D **85** (2012), 035014 [arXiv:1104.1387 [hep-ph]].
- [48] M. E. Gómez, T. Hahn, S. Heinemeyer and M. Rehman, Phys. Rev. D **90** (2014) no.7, 074016 [arXiv:1408.0663 [hep-ph]].
- [49] M. E. Gomez, S. Heinemeyer and M. Rehman, J. Part. Phys. **1** (2017) no.1, 30-50 [arXiv:1703.02229 [hep-ph]].
- [50] B. C. Allanach, C. Balazs, G. Belanger, M. Bernhardt, F. Boudjema, D. Choudhury, K. Desch, U. Ellwanger, P. Gambino and R. Godbole, *et al.* Comput. Phys. Commun. **180** (2009), 8-25 [arXiv:0801.0045 [hep-ph]].
- [51] J. Beuria and A. Dey, JHEP **10** (2017), 154 [arXiv:1708.08361 [hep-ph]].
- [52] E. Bagnaschi *et al.*, Eur. Phys. J. C **79** (2019) no.7, 617 [arXiv:1808.07542 [hep-ph]].
- [53] P. Slavich, S. Heinemeyer (eds.), E. Bagnaschi *et al.*, Eur. Phys. J. C **81** (2021) no.5, 450 [arXiv:2012.15629 [hep-ph]].
- [54] G. Aad *et al.* [ATLAS], Phys. Rev. Lett. **125** (2020) no.5, 051801 [arXiv:2002.12223 [hep-ex]].
- [55] A. Tumasyan *et al.* [CMS], JHEP **07** (2023), 073 [arXiv:2208.02717 [hep-ex]].
- [56] G. Aad *et al.* [ATLAS], [arXiv:2402.05742 [hep-ex]].

- [57] R. L. Workman *et al.* [Particle Data Group], PTEP **2022** (2022), 083C01
- [58] G. Aad *et al.* [ATLAS], Phys. Lett. B **801** (2020), 135148 doi:10.1016/j.physletb.2019.135148 [arXiv:1909.10235 [hep-ex]].
- [59] A. M. Baldini *et al.* [MEG II], Eur. Phys. J. C **78** (2018) no.5, 380 [arXiv:1801.04688 [physics.ins-det]].
- [60] Q. Qin, Q. Li, C. D. Lü, F. S. Yu and S. H. Zhou, Eur. Phys. J. C **78** (2018) no.10, 835 [arXiv:1711.07243 [hep-ph]].
- [61] E. Kou *et al.* [Belle-II], PTEP **2019** (2019) no.12, 123C01 [erratum: PTEP **2020** (2020) no.2, 029201]